UNIVERSITY OF COPENHAGEN



Københavns Universitet

Establishing heterologous betaxanthin pigment biosynthesis in cyanobacteria

Hanamghar, Sayali S.; Russo, David A.; Mellor, Silas Busck; Zedler, Julie A. Z.

Published in:
Metabolic Engineering

DOI:
10.1016/j.ymben.2026.01.002

Publication date:
2026

Document license:
CC BY

Citation for published version (APA):
Hanamghar, S. S., Russo, D. A., Mellor, S. B., & Zedler, J. A. Z. (2026). Establishing heterologous betaxanthin pigment biosynthesis in cyanobacteria. *Metabolic Engineering*, *94*, 264-272. https://doi.org/10.1016/j.ymben.2026.01.002

Download date: 05. Oct. 2026

Metabolic Engineering 94 (2026) 264–272

Contents lists available at ScienceDirect

Metabolic Engineering

journal homepage: www.elsevier.com/locate/meteng

Establishing heterologous betaxanthin pigment biosynthesis in cyanobacteria

Sayali S. Hanamghar [a,1], David A. Russo [b,1], Silas Busck Mellor [c], Julie A.Z. Zedler [a,*]

[a] Friedrich Schiller University Jena, Matthias Schleiden Institute for Genetics, Bioinformatics and Molecular Botany, Synthetic Biology of Photosynthetic Organisms, D-07743, Jena, Germany
[b] Friedrich Schiller University Jena, Institute for Inorganic and Analytical Chemistry, Bioorganic Analytics, D-07743, Jena, Germany
[c] Department of Plant and Environmental Sciences, University of Copenhagen, DK-1871, Frederiksberg, Denmark

ARTICLE INFO

Keywords:
Betalain
Betaxanthin
Cyanobacteria
Cytochrome P450
Shikimate pathway
Synechocystis

ABSTRACT

Betalains are water-soluble pigments with two major classes: red-violet betacyanins and yellow-orange betaxanthins. These pigments are increasingly being sought after as natural replacements for synthetic pigments in the food industry. Traditionally, betalains are extracted from cultivated plants. But due to low concentrations of native pigments, the process is inherently inefficient. Now, an increase in consumer demand calls for the development of scalable and sustainable betalain production routes. To address this challenge, we introduced a heterologous pathway for the production of betaxanthins into cyanobacteria. The pathway consists of an engineered variant of the cytochrome P450 CYP76AD1 (W13L, F309L) and the L-DOPA 4,5-dioxygenase DODA1 from *Beta vulgaris* (beet). Introduction of the two-enzyme betaxanthin pathway in *Synechocystis* sp. PCC 6803 did not result in detectable betaxanthins. Subsequent metabolic adjustments to the shikimate pathway, using a feedback resistant $AroG^{fbr}$ from *E. coli*, led to an overaccumulation of the aromatic amino acids phenylalanine, tryptophan, and tyrosine, and the production of low levels of phenylalanine-betaxanthin. Optimization of the cultivation conditions (i.e., growth in nutrient-rich medium and CO_2-enriched air) increased titers approximately 165 times and led to the production of phenylalanine-betaxanthin with a final titer of 18.2 ± 5.1 mg L^{-1}. Our work establishes a microbial system for photoautotrophic betaxanthin pigment production without the need for exogenous amino acid supplementation.

1. Introduction

Betalains are water-soluble red-violet and yellow-orange pigments that contain nitrogen. They mostly occur in members of the plant order Caryophyllales such as *Beta vulgaris* (Timoneda et al., 2019), *Amaranthus tricolor* (Chang et al., 2021) and *Dianthus caryophyllus* (Sadowska-Bartosz and Bartosz, 2021). These pigments are also produced in fungi (Babos et al., 2011; Hinz et al., 1997) and the bacterium *Gluconacetobacter diazotrophicus* (Contreras-Llano et al., 2019). Betalains have applications in the pharmaceutical and nutraceutical industries due to their antioxidant and anti-inflammatory properties. They are also widely used in the food industry as a red food colorant and are being tested as ammonia indicator dyes in smart food packaging (Abedi-Firoozjah et al., 2023; Sadowska-Bartosz and Bartosz, 2021).

Betalain biosynthesis starts with tyrosine (Tyr), which is hydroxylated to L-3,4-dihydroxyphenylalanine (L-DOPA) by the cytochrome P450 CYP76AD1 (Polturak et al., 2016) (Fig. S1). This cytochrome P450 enzyme is also responsible for the oxidation of L-DOPA to L-dopaquinone which spontaneously cyclizes to cyclo-DOPA (Hatlestad et al., 2012). In the second step, 4,5-DOPA-extradiol-dioxygenase (DODA1) catalyzes the ring-opening oxidation of L-DOPA to form the instable intermediate 4,5-seco-dopa that spontaneously cyclizes into betalamic acid, the common chromophore of betalains (Fernando Gandía-Herrero and García-Carmona, 2012). Betalamic acid can spontaneously condense with amines and their derivatives to form betaxanthins. Betalamic acid can also spontaneously condense with cyclo-DOPA and/or its glucosyl

* Corresponding author. Friedrich Schiller University Jena, Matthias Schleiden Institute for Genetics, Bioinformatics and Molecular Botany, Synthetic Biology of Photosynthetic Organisms, Philosophenweg 12, 07743, Jena, Germany.
E-mail addresses: sayali.hanamghar@uni-jena.de (S.S. Hanamghar), david.russo@uni-jena.de (D.A. Russo), silasmellor@plen.ku.dk (S.B. Mellor), julie.zedler@uni-jena.de (J.A.Z. Zedler).
[1] S. S. Hanamghar and D.A. Russo contributed equally.

https://doi.org/10.1016/j.ymben.2026.01.002
Received 2 July 2025; Received in revised form 30 December 2025; Accepted 5 January 2026
Available online 5 January 2026
1096-7176/© 2026 The Authors. Published by Elsevier Inc. on behalf of International Metabolic Engineering Society. This is an open access article under the CC BY license (http://creativecommons.org/licenses/by/4.0/).

Table 1
Synechocystis sp. PCC 6803 strains generated in this study.

Strain ID	Plasmid	Description
Syn-N^{Kan}	pPMQAK1-T (Vasudevan et al., 2019)	*Synechocystis* sp. PCC 6803 carrying self-replicative shuttle plasmid (CyanoGate Kit), (Vector ID pCAT.000); no gene of interest, selection markers: Ampicillin, Kanamycin.
Syn-Bx	pSH023 (this study)	*Synechocystis* sp. PCC 6803 carrying plasmid with promoter P_{RhaBAD} - Bx operon (*CYP76AD1^{mut}-HA, BvDODA1-HA*) - terminator T_{cpc_operon}; promoter P_{J23116} - *rhaS* - terminator T_{cpc_operon}; backbone: pPMQAK1-T.
Syn-Bx^{AroG*}	pSH018 (this study)	*Synechocystis* sp. PCC 6803 carrying plasmid with promoter P_{RhaBAD} - Bx operon (*CYP76AD1^{mut}-HA, BvDODA1-HA*) - terminator T_{cpc_operon}; promoter P_{J23116} -*aroG^{fbr}-His, rhaS* - terminator T_{cpc_operon}; backbone: pPMQAK1-T.

CYP76AD1^{mut}: mutated gene sequence encoding CYP76AD1 variant (W13L, F309L) (DeLoache et al., 2015).

derivatives to form betacyanins (Fig. S1). Betaxanthins are yellow-colored pigments with absorption maxima between 460 and 480 nm that exhibit strong fluorescence due to the structural properties of the betalamic acid moiety bound to an amine group (Spórna-Kucab et al., 2023). Betacyanins, on the other hand, are weakly fluorescent red and violet pigments with two absorption maxima; one in the UV range between 270 and 280 nm and one in the visible range between 535 and 540 nm (Azeredo, 2009).

Heterologous betalain biosynthesis has previously been established in crop plants (Grützner et al., 2021; Polturak et al., 2017; Wang et al., 2024) and heterotrophic microbial hosts such as *Escherichia coli* (Guerrero-Rubio et al., 2019; Hou et al., 2020) and *Saccharomyces cerevisiae* (Babaei et al., 2023; DeLoache et al., 2015). Amongst the betalains, betaxanthins are particularly interesting owing to their strong antioxidant and bioactive potential (Khan, 2016). However, titers in *E. coli* and yeast are typically lower than those of betacyanins due to the relative insolubility of some amino acids and a short half-life of around 3 h for most betaxanthins (Esteves et al., 2025). Consequentially, amino acid betaxanthin titers produced in heterotrophic monocultures are modest and range from 11 to 208 mg L^{-1} (Guerrero-Rubio et al., 2019; Xue et al., 2025). Moreover, the exogenous addition of carbon sources, amino acids, and stabilizers, such as ascorbic acid, is often required to achieve these titers.

The aim of this study was, therefore, to establish the production of betaxanthins in a photoautotrophic microbial host. Cyanobacteria are prokaryotes that perform oxygenic photosynthesis. In recent years, there has been increasing evidence of the potential of cyanobacteria as whole cell catalysts. This is particularly the case for industrially relevant redox reactions that are often limited by NAD(P)H availability in heterotrophic hosts. In cyanobacteria, the rate-limiting dependence on NAD(P)H can be circumvented by taking advantage of the excess reducing power generated by photosynthesis for light-driven catalysis (Jodlbauer et al., 2021; Russo et al., 2019a; Toepel et al., 2023). Furthermore, functional expression of membrane-bound cytochrome P450s is known to be challenging in established heterotrophic systems such as yeast (Jiang et al., 2021) and *E. coli* (Shang et al., 2023). Cyanobacteria have previously been shown to have a high potential for functional cytochrome P450 expression of membrane-bound (Berepiki et al., 2016; Lassen et al., 2014; Mascia et al., 2022) and soluble cytochrome P450 enzymes (Hoschek et al., 2019).

In this study we use the cyanobacterium *Synechocystis* sp. PCC 6803 (Syn6803) as a host to express an engineered variant of *CYP76AD1* and *BvDODA1*, the two genes that constitute the biosynthetic pathway for betaxanthin production in *Beta vulgaris*. We show that sole expression of the betaxanthin pathway was not sufficient to produce betaxanthins to a detectable level. The addition of a feedback-resistant *aroG* (*aroG^{fbr}*) increased the phenylalanine (Phe), tryptophan (Trp) and Tyr pools and led to the detection of Phe-betaxanthin (Phe-Bx). Subsequent high-density photoautotrophic cultivation improved Phe-Bx production approximately 165 times to a final yield of 18.2 ± 5.1 mg L^{-1}. Our work provides the first demonstration of betalain production in a photoautotrophic microbe.

2. Materials and methods

2.1. Cyanobacterial strains and cultivation conditions

A glucose-tolerant, non-motile *Synechocystis* sp. PCC 6803 sub-strain "Kaplan" was used. Cultures were maintained at 30 °C with approximately 50 μmol photons m^{-2} s^{-1} continuous illumination on 1.5 % agar plates of BG-11 medium (Stanier et al., 1971) supplemented with 5 mM 4-(2-Hydroxyethyl)piperazine-1-ethanesulfonic acid (HEPES) (pH 7.5) and 3 g L^{-1} sodium thiosulfate pentahydrate. Liquid cultures were grown in BG-11 supplemented with HEPES ($BG\text{-}11_H$) in 50 mL tissue flasks (Greiner, product no.: 690175) at 30 °C with continuous illumination (approximately 50 μmol photons m^{-2} s^{-1}) and shaking at 125 rpm. Engineered strains were supplemented with 50 μg mL^{-1} kanamycin for plasmid maintenance on $BG\text{-}11_H$ agar plates and in liquid culture.

All experiments in liquid culture were inoculated in triplicate to an optical density (OD) at 750 nm of 0.5 in 50 mL $BG\text{-}11_H$ supplemented with 50 μg mL^{-1} kanamycin. Cultures were induced with 1 mg mL^{-1} L (+)-rhamnose monohydrate (Carl-Roth) after 24 h of growth. Samples were harvested every 24 h to measure the OD and extract pigments.

The high-density cultivation experiment was carried out in a HDC 6.10 cultivation setup (CellDeg) in P4-TES CPH medium as previously described (Russo et al., 2022) with small modifications: the cultures were supplemented with 50 μg mL^{-1} kanamycin and induced with 1 mg mL^{-1} rhamnose after 24 h of growth. HDC culture vessels were agitated by shaking at 250 rpm.

2.2. Construction of plasmids

All cloning was performed in *E. coli* NEB 5-alpha (New England Biolabs) for plasmid propagation. Plasmids were generated by Golden-Gate cloning using the CyanoGate syntax (Vasudevan et al., 2019). The self-replicating plasmid pPMQAK1-T (Addgene kit #1000000146, gift from Alistair McCormick) was used for final construct assembly in Level T. For domestication (removal of internal BbsI recognition sites in *BvDODA1* gene) and generation of individual CyanoGate-compatible parts, DNA sequences were either amplified from existing plasmids or custom-synthesized as double stranded DNA fragments (gBlock, Integrated DNA Technologies). BbsI recognition sites were added for Level 0 part generation by PCR with Q5® Hot start High-Fidelity DNA Polymerase (New England Biolabs). Primers sequences used for individual part generation are shown in Table S1 (Supplementary Material). GoldenGate assemblies were performed using a standard protocol (Weber et al., 2011) with small modifications: assembly reactions were incubated in a thermocycler with 30 cycles of restriction enzyme activation (BbsI-HF or BsaI-HFv2, New England Biolabs) at 37 °C for 5 min followed by activation of the T4 DNA ligase for 5 min at 16 °C. A final restriction enzyme inactivation step was added at 85 °C for 20 min. Level 0 and final Level T constructs were verified using Sanger sequencing (Eurofins Genomics) and colony PCR. Plasmid maps of generated level T shuttle vectors (Table 1) are deposited on Zenodo at https://doi.org/10.5281/zenodo.15673972. All gene sequences used in this study are also listed in Table S2.

2.3. Generation of cyanobacterial strains

Plasmids were transferred into cyanobacterial recipient strains by triparental mating as described previously (Zedler et al., 2023) and selected on BG-11_H agar plates with 50 μg mL^{-1} kanamycin. The presence of target plasmids in colonies was verified by colony PCR. DNA from colonies was extracted by boiling of a single colony resuspended in 50 μL of ddH_2O at 95 °C for 10 min. Subsequently, 2 μL of the DNA extract were used in a PCR reaction with primers specified in Table S1. An overview of all generated strains from this study is shown in Table 1.

2.4. Preparation of whole cell lysates and determination of protein content

Whole cell lysates were prepared as previously described (Russo et al., 2019b) with the exception that an equivalent of OD = 10 was harvested after 9 days of cultivation and lysed in 0.5 mL of lysis buffer. The protein content of cleared cell lysates was estimated with a Pierce bicinchoninic acid protein assay kit (Thermo Fisher Scientific) in a 96-well plate format.

2.5. SDS-PAGE and immunoblotting

An equivalent of 10 μg total protein extracted from cleared cell lysates was denatured at 50 °C for 10 min in sample loading buffer (containing 2 % SDS and 0.1 M dithiothreitol). Proteins were subsequently separated on a 4–12 % Criterion™ XT Bis-Tris Protein Gel (Bio-Rad Laboratories), using 3-(N-morpholino) propanesulfonic acid (MOPS) as the running buffer, at 100 V. Proteins were then transferred onto a 0.45-μm pore size nitrocellulose membrane using a Trans-Blot® Turbo transfer system (Bio-Rad Laboratories) for immunoblotting. Membranes were blocked with 5 % skimmed milk powder (w/v) in TBS-T buffer (10 mM Tris-HCl (pH 8.0), 150 mM NaCl, and 0.05 % Tween 20) for 60 min at room temperature. The nitrocellulose membrane was either incubated with an anti-HA antibody produced in rabbit (dilution 1:5000, Sigma-Aldrich, product no.: H6908) or an anti-His antibody produced in mouse (dilution 1:1000, Novagen, product no.: 70796) overnight at 4 °C. Membranes were washed three times with TBS-T and incubated for 60 min at room temperature with an anti-rabbit or anti-mouse HRP-conjugated secondary antibody (Promega) at a 1:5000 dilution. After three more wash steps in TBS-T, the chemiluminescent signal was developed using a Clarity Max Western ECL Substrate (Bio-Rad Laboratories). Chemiluminescence was detected using a ChemiDoc imager (Bio-Rad Laboratories).

2.6. Fluorescence measurements in culture supernatants

The supernatant from cultures was harvested by centrifugation at 9300×*g* for 5 min at 4 °C. A volume of 100 μL culture supernatant was transferred to black 96-well plates. Fluorescence measurements were recorded in a VANTAstar® plate reader (BMG Labtech) with the excitation set to 475 nm and emission measured at 515 nm. A bandwidth of 15 nm (excitation and emission) with a focal height of 5 mm and a fixed gain of 1000 were used. Significance was tested with a multiple unpaired Student's t-test and the false discovery rate (FDR) was controlled by the Benjamini-Krieger-Yekutieli two-stage procedure.

2.7. L-DOPA feeding assay

For L-3,4-Dihydroxyphenylalanine (L-DOPA, Sigma-Aldrich) feeding experiments, two sets of cultures were grown and induced with 1 mg mL^{-1} rhamnose after 24 h. After 48 h, L-DOPA and ascorbic acid were added to one set of cultures at a final concentration of 100 μM L-DOPA and 0.34 mM ascorbic acid. As a control, the equivalent volume of fresh medium was added to the other set. An L-DOPA stock solution (10 mM L-DOPA and 34 mM ascorbic acid in ddH_2O) was prepared fresh for each experiment. Significance was tested with a multiple unpaired Student's t-test and the FDR was controlled by the Benjamini-Krieger-Yekutieli two-stage procedure.

2.8. Pigment analysis

Chlorophyll *a* and carotenoid content of samples was determined by methanol extraction from frozen pellets as previously described (Russo et al., 2019b). Pigment content in mg L^{-1} was calculated for chlorophyll *a* (Ritchie, 2006) and total carotenoids (Myers et al., 1980).

2.9. Semi-synthesis of a phenylalanine-betaxanthin standard

A semi-synthetic Phe-Bx standard was prepared in-house following a previously established method (Cabanes et al., 2014) with several modifications. Two grams of commercial *Beta vulgaris* (beet) powder were dissolved in 20 mL ddH_2O. The mixture was then filtered with a 125 μm E-D-SCHNELLSIEB® nylon filter to remove remaining insoluble debris. Subsequently, 2 g of Lewatit VP OC 1065 (Sigma-Aldrich) were added to the filtrate and the pH titrated to pH 11.4 with aqueous ammonia. After a 10 min incubation step with constant stirring at room temperature, the pH was reduced to 5.0 with glacial acetic acid. The mixture was incubated for 30 min with constant stirring. Lewatit beads were then collected on a filter and thoroughly rinsed first with ddH_2O followed by methanol. The beads were then carefully dried under a nitrogen gas stream. Beads were resuspended in aqueous ammonia and incubated for 30 min at pH 11.4. Following the addition of 500 mg Phe, the pH of the solution was adjusted to 5.0 with glacial acetic acid. The condensation product was stirred for another 30 min before storage at −20 °C or −80 °C until further use. Before use, the standard was quantified by UV–vis absorption spectrophotometry using a molar absorption coefficient at 480 nm of 4.8 x 10^4 L^{-1} mol^{-1} cm^{-1}. A dilution series of the standard was then prepared to generate calibration curves using 0.31–5 μM (tissue flask experiment) (Fig. S2A) and 0.31–9.85 μM (high-density experiment) concentrations (Fig. S2B). When stereoisomers were present, the sum of both peaks was used for calculations. Goodness-of-fit of the linear model was judged based on the coefficient of determination (R^2). Retention times of Phe-Bx were 10.6 and 11.25 min. The limit of detection (LOD) was calculated with the expression 3.3σ/S where σ is the standard deviation of the residuals and S is the slope of the calibration curve. The limit of quantification (LOQ) was calculated with the expression 10σ/S. The LOD for Phe-Bx was 0.32 μM (tissue flask experiment) and 0.52 μM (high-density experiment). The LOQ for Phe-Bx was 0.98 μM (tissue flask experiment) and 1.57 μM (high-density experiment). Selected calibration parameters are reported in Table S3. Phe-Bx samples were always measured together with their respective standard curves to mitigate inter-batch variability. To evaluate ion suppression of the P4-TES CPH medium, the Phe-Bx standard was added to either conditioned P4-TES CPH medium (Syn-N^{Kan}, day 5 high-density experiment) or ddH_2O (approximately 12 μM final concentration). Based on this analysis, a correction factor of 1.35 was applied to measurements in P4-TES CPH medium (Fig. S3).

2.10. Liquid chromatography mass spectrometry (LC-MS)

For LC-MS analysis, the culture medium was harvested by centrifugation at 9300×*g*, 5 min at 4 °C and samples were stored at −80 °C until analysis. Ultra-high-performance LC coupled with high resolution MS was carried out using a Vanquish UHPLC system (Thermo Fisher Scientific) with a VF-P10-A binary pump and a VF-A10-A auto sampler which was set to 10 °C and equipped with a 25 μL injection syringe and a 100 μL sample loop. The column, Accucore® C-18 RP (100 × 2.1 mm; 2.6 μm, Thermo Fisher Scientific), was kept at 25 °C within the column compartment VH-C10-A. Eluent A was water with 2 % acetonitrile and 0.1 % formic acid. Eluent B was pure acetonitrile. All solvents and water were LC-MS grade. The gradient for sample separation started with 0 %

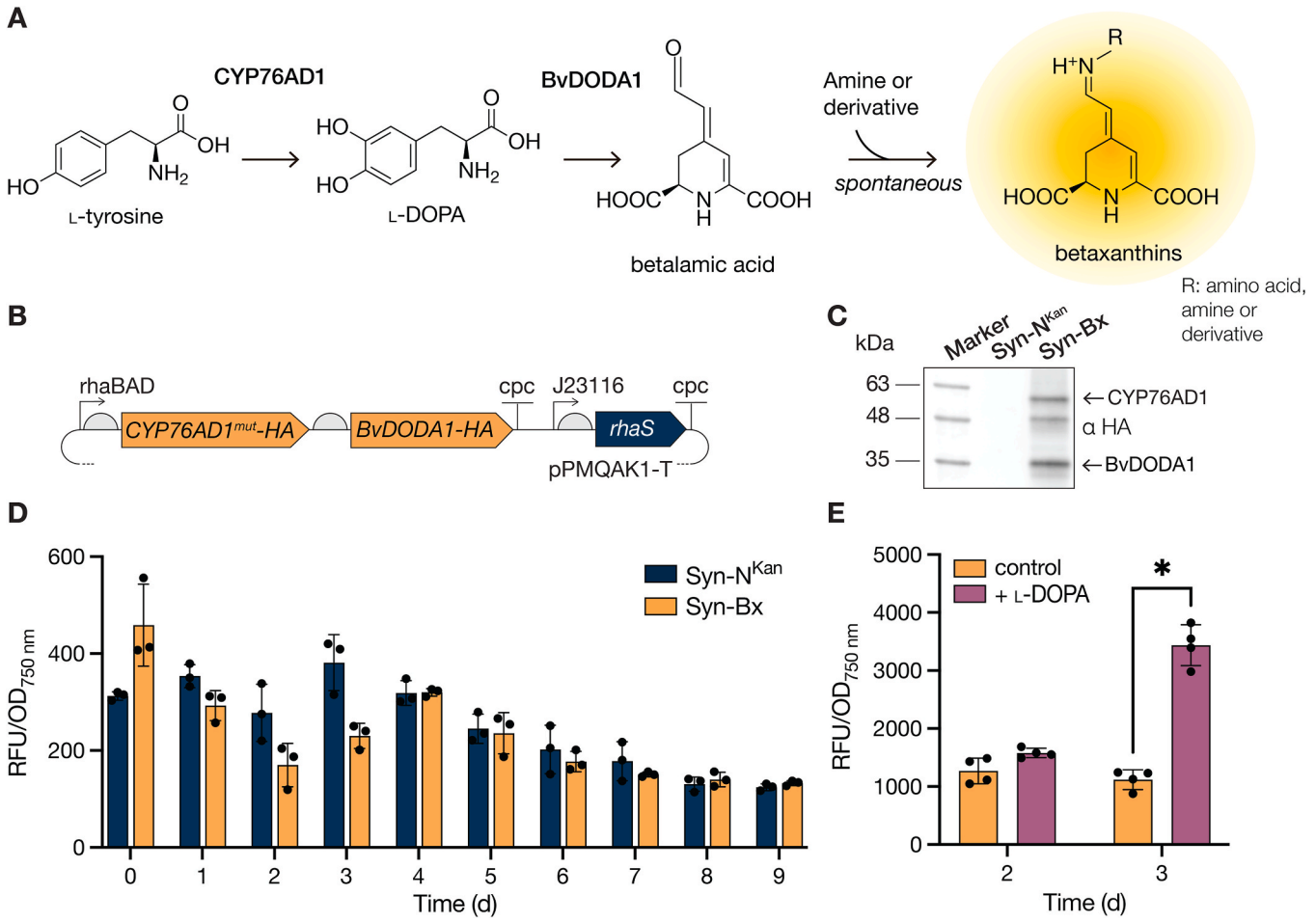


Fig. 1. Engineering of a minimal pathway for betaxanthin biosynthesis in Syn6803. **A** Overview of the Bx pathway in *Beta vulgaris*. **B** Construct design for extrachromosomal expression of a Bx operon (*CYP76AD1^{mut}-HA* and *BvDODA1-HA)* under the control of the rhaBAD promoter. The open reading frame *CYP76AD1^{mut}-HA* encodes an engineered variant (W13L, F309L) of CYP76AD1 fused with a C-terminal HA-tag. The transcription factor-encoding gene *rhaS* was expressed from the same vector with a constitutive J23116 promoter. **C** Immunodetection of CYP76AD1 and BvDODA1 in cleared cell lysates with an anti-HA antibody (αHA). **D** OD-normalized fluorescence (Ex: 475/15, Em: 515/15) of culture medium measured over 9 days of cultivation. Cultures were induced at day 1. Bars show averages (n = 3), error bars: ±SD. **E** OD-normalized fluorescence (Ex: 475/15, Em: 515/15) of culture medium of Syn-Bx with (+L-DOPA) and without the addition of L-DOPA (control) after 2 days of growth. Bars show averages (n = 4), error bars: ±SD. Syn-Bx denotes the strain engineered for betaxanthin biosynthesis, Syn-N^{Kan} is a negative control strain carrying the plasmid pPMQAK1-T.

B to 2.2 min, followed by an increase to 11 % B over 10 min, and 90 % B over a further 4 min. It was then kept at 90 % B for 2 min and re-equilibrated to 0 % B over 1 min. Flow rate was kept constant at 0.5 mL min^{-1}. The Vanquish UHPLC system was also equipped with a variable wavelength detector (VC-D40-A-01). UV–Vis data were collected from 190 to 680 nm with a bunch width of 1 nm. The sample injection volume was 1 μL. Mass spectra were recorded with an Orbitrap Exploris 480 MS (Thermo Fisher Scientific) coupled to a heated electrospray (HESI) source. For monitoring, two full scan modes were selected with the following parameters: Polarity: positive; scan range (*m/z*): 100 to 1500; resolution: 180,000; AGC target: standard; maximum injection time mode: auto. General settings: sheath gas flow rate (arb): 50; auxiliary gas flow rate (arb): 10; sweep gas flow rate (arb): 1; spray voltage (kV): 3.5; capillary temperature (°C): 325; RF lens (%): 50; vaporizer temperature (°C): 350; acquisition time (min): 0.7–16.2. Data analysis and peak area calculation were done on Freestyle 1.8 SP2 (Thermo Fisher Scientific). The metabolomics data have been deposited to the MetaboLights (Yurekten et al., 2024) repository with the study identifier MTBLS12639.

2.11. LC-MS measurement of phenylalanine, tyrosine and tryptophan

For measurement of Phe, Tyr, and Trp levels, a culture volume of 300 μL was harvested daily and the cells were separated by centrifugation at 9300×*g* for 5 min at 4 °C. Before storage, the cell pellets were washed with 300 μL of their respective growth medium. All samples were stored at −80 °C until the analysis. For measurement of intracellular levels, cell pellets were resuspended in 200 μL 50 % aqueous MeOH (v/v) and sonicated on ice for 10 min. The suspension was then centrifuged for 2 min at 14, 000×*g* and the supernatant was used for LC-MS analysis. The difference between the harvested culture volume (300 μL) and the resuspension volume (200 μL) was accounted for in the final calculations. For measurement of extracellular levels, the supernatant was thawed shortly before the analysis and used without further modification or, when necessary, diluted appropriately with P4-TES CPH medium. To relate chromatographic areas with compound concentrations, calibration curves were performed for the amino acids Phe (0.16–10 μM for the low range and 1.56–100 μM for the high range), Tyr (0.16–10 μM for the low range and 1.56–50 μM for the high range), and Trp (0.39–25 μM for the low range and 3.91–250 μM for the high range) (Fig. S4). Goodness-of-fit of the linear model was judged based on the coefficient of determination (R^2). Retention times were as follows: Tyr

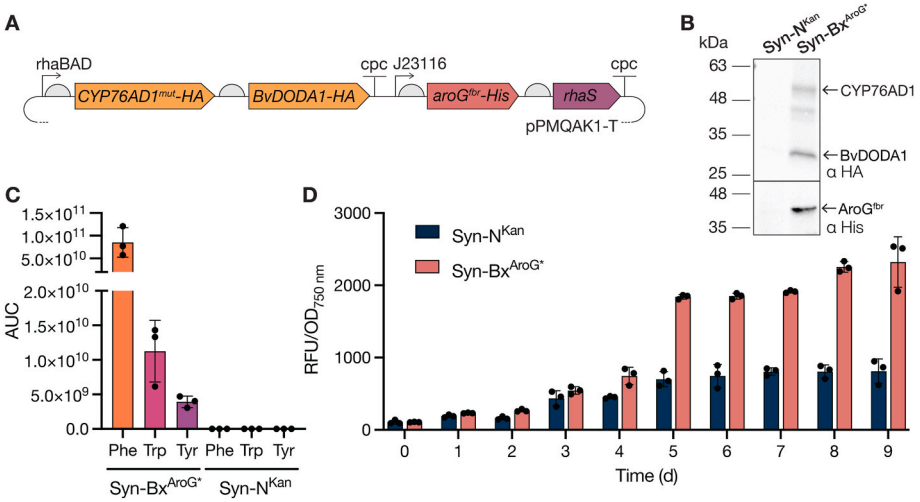


Fig. 2. Co-expression of *aroG*^{fbr} increases the aromatic amino acid pool in a betaxanthin producing Syn6803. **A** Construct design for co-expression of a Bx operon in conjunction with a pJ23116-controlled feedback-resistant *aroG*^{fbr}. *CYP76AD1*^{mut}: engineered variant (W13L, F309L) of CYP76AD1. **B** Immunodetection of CYP76AD1 and BvDODA1 with an anti-HA antibody (αHA) and AroG^{fbr}-His detection with an anti-His antibody (αHis) in cleared cell lysates. **C** LC-MS evidence of amino acids phenylalanine (Phe), tryptophan (Trp) and tyrosine (Tyr) in the culture medium. Bars show averages (n = 3), error bars: ±SD. **D** OD-normalized fluorescence (Ex: 475/15, Em: 515/15) of culture medium measured over 9 d of cultivation. Cultures were induced at day 1. Bars show averages (n = 3), error bars: ±SD. Syn-Bx^{AroG*} denotes the strain engineered for Bx biosynthesis with AroG^{fbr}, Syn-N^{Kan} is a negative control strain carrying the plasmid pPMQAK1-T.

= 0.53 min, Phe = 0.59 min, and Trp = 2.7 min. LODs were calculated in the same way as for Phe-Bx and were as follows: Phe = 15.11 μM (high range) and 1.07 μM (low range), Tyr = 7.2 μM (high range) and 1.64 μM (low range) and Trp = 11.29 μM (high range) and 1.17 μM (low range). LOQs were calculated in the same way as for Phe-Bx and were as follows: Phe = 45.80 μM (high range) and 3.24 μM (low range), Tyr = 21.81 μM (high range) and 4.98 μM (low range) and Trp = 34.20 μM (high range) and 3.55 μM (low range). Selected calibration parameters are reported in Table S3.

3. Results

3.1. Precursor availability limits betaxanthin production in Synechocystis sp. PCC 6803

In *Beta vulgaris*, two enzymes are required for Bx biosynthesis: a cytochrome P450 (CYP76AD1, UniProtKB: I3PFJ5), that hydroxylates Tyr to L-DOPA, and a L-DOPA dioxygenase (BvDODA1, UniProtKB: I3PFJ9), which converts L-DOPA into betalamic acid. Betalamic acid can then spontaneously condense with amines and amino acids to form Bx (Fig. 1A, Fig. S1). CYP76AD1 also catalyzes the first step in the conversion of L-DOPA to cyclo-DOPA (i.e., production of L-dopaquinone). Cyclo-DOPA can then condense with betalamic acid to form violet-colored betanidin (Fig. S1). The CYP76AD1 variant (W13L, F309L) previously showed suppressed L-dopaquinone production and, consequentially, enhanced betaxanthin production (DeLoache et al., 2015). To establish a Bx pathway in cyanobacteria, genes encoding C-terminally HA-tagged variants of CYP76AD1 (W13L, F309L) (57.1 kDa) and BvDODA1 (32.2 kDa) were expressed in Syn6803 (hereafter, Syn-Bx) under the control of the rhamnose-inducible *rhaBAD* promoter. For prhaBAD transcriptional activation, the regulator RhaS was co-expressed under the control of the constitutive low-to-medium strength J23116 promoter (Fig. 1B, Table 1). Successful transfer of the self-replicative plasmid was confirmed by colony PCR (Fig. S5). To determine whether the two proteins were produced, cultures of Syn-Bx were induced with rhamnose and grown for protein analysis by immunoblotting. The presence of CYP76AD1 and BvDODA1 in Syn-Bx cleared cell lysates was confirmed at the predicted molecular weights of 57 kDa and 32 kDa, respectively (Fig. 1C). An additional band around 50 kDa was consistently observed only in the Syn-Bx strain. Based on the size difference to the mature CYP76AD1 enzyme, this band could derive from cleavage of the transmembrane domain (Fig. 1C). In microbial production systems, betaxanthins are known to accumulate in the medium (Guerrero-Rubio et al., 2019). Therefore, medium samples were harvested from cultures every 24 h to determine if betaxanthins were produced in Syn-Bx. Taking advantage of the intrinsic betaxanthin fluorescence, we conducted a fluorescence analysis using previously determined excitation and emission maxima for betaxanthins (Gandía-Herrero et al., 2005a). This did not provide any indication of betaxanthin accumulation (Fig. 1D). Overall, our results showed that CYP76AD1 and BvDODA1 were produced in Syn-Bx, however no detectable amount of betaxanthin could be measured.

To troubleshoot the lack of betaxanthin production, we started by investigating whether the first step of the pathway, namely the conversion of Tyr to L-DOPA by CYP76AD1, was the bottleneck. To test this, an induced Syn-Bx culture was grown for 2 d and fed with 100 μM L-DOPA. The normalized fluorescence values were approximately three times higher in L-DOPA-fed cultures when compared to their counterparts where no L-DOPA was added (Fig. 1E). To identify the main betaxanthin responsible for the increased fluorescence levels, the culture medium was analyzed by LC-MS. Despite a thorough search using the monoisotopic masses of betalamic acid and all 20 amino acid betaxanthins (Esteves et al., 2022), neither betalamic acid nor betaxanthins were identified. One possible explanation is that betalamic acid spontaneously condensed with multiple, readily available, amino acids or amines and no dominant product emerged, thus complicating the identification of the specific betaxanthins formed.

3.2. Overproduction of tyrosine and phenylalanine leads to the accumulation of phenylalanine-betaxanthin

Our previous results suggested that the betaxanthin pathway was functional in Syn6803 but limited by L-DOPA availability. Therefore, we hypothesized that the L-DOPA limitation could derive from insufficient Tyr supply to CYP76AD1 (Fig. 1A). To test this hypothesis, a feedback-resistant *aroG* (*aroG*^{fbr}) from *E. coli* was added in an operon with the transcription factor *rhaS* to the Bx plasmid (Fig. 2A, Table 1). AroG is a 3-deoxy-D-arabino-heptulosonate-7-phosphate (DAHP) synthase that catalyzes and regulates one of the first steps of the shikimate pathway. While AroG is typically inhibited by Phe, in AroG^{fbr} the amino acid

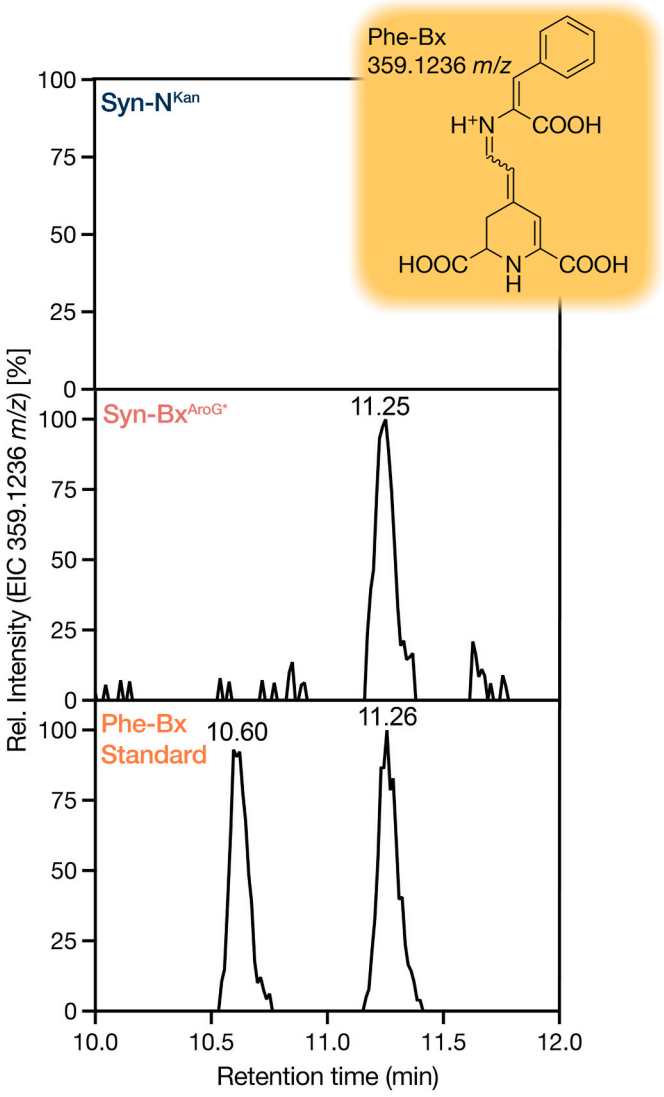


Fig. 3. LC-MS evidence of phenylalanine-betaxanthin (Phe-Bx) production in the Syn-Bx^{AroG*} strain. Extracted ion chromatograms (EIC) of the negative control strain Syn-N^{Kan} (top), Syn-Bx^{AroG*} (center), both at day 5, and 5 μM of the Phe-Bx semi-synthetic standard (bottom). The structural formula of Phe-Bx and its associated monoisotopic mass in positive ion mode are shown in the inset.

residues responsible for the feedback inhibition have been mutated. In a previous study, expression of *aroG*^{fbr} in Syn6803 led to a 100 times increase in Phe concentrations, and 10 times increase in Tyr and Trp concentrations (Brey et al., 2020).

The generated plasmid was conjugated into Syn6803 to generate the strain Syn-Bx^{AroG*} (Fig. 2). Successful strain generation was validated by colony PCR (Fig. S5). Cultures of the Syn-Bx^{AroG*} strain were then grown for immunoblot and product analysis. Immunoblot analysis of the Syn-Bx^{AroG*} cleared cell lysates confirmed the presence of all three proteins CYP76AD1, BvDODA1 and AroG^{fbr} (Fig. 2B). Growth analysis showed that, in comparison to the negative control strain and the Syn-Bx strain, Syn-Bx^{AroG*} entered stationary phase earlier and achieved an approximately 30 % lower final OD (Fig. S6A). This was supported by pigment content analysis which showed that the chlorophyll *a* concentrations of Syn-Bx^{AroG*} were approximately 25–35 % lower in comparison to the other two strains throughout most of the experiment (Fig. S6B). On the other hand, carotenoid concentrations were similar among all strains (Fig. S6C).

It was expected that the presence of AroG^{fbr} would increase the amount of Phe, Tyr, and Trp, therefore we searched for chromatographic signals of these three amino acids in the culture medium of Syn-Bx^{AroG*}. An excess of Phe, Tyr, and Trp could be detected, thus suggesting that AroG^{fbr} was functional (Fig. 2C). This was also reflected in a subsequent betaxanthin fluorescence analysis. Normalized fluorescence of the Syn-Bx^{AroG*} culture medium was significantly higher than that of Syn-N^{Kan} from day 4 ($p = 0.01$) until the end of the experiment ($p < 0.001$), suggesting the formation of betaxanthins (Fig. 2D). Normalized fluorescence spiked at day 5 and gradually increased until day 9 (Fig. 2D). Therefore, culture medium harvested at days 5 and 9 was further analyzed by LC-MS.

We searched for chromatographic signals of betaxanthins derived from condensation of betalamic acid with the overproduced aromatic amino acids (Phe, Trp, Tyr) in the Syn-Bx^{AroG*} culture medium. However, only Phe-Bx could be putatively identified. The identity of Phe-Bx was confirmed by comparing the associated retention time and mass with those of a semi-synthetic standard (Fig. 3). The two peaks observed in the reference standard correspond to the 2*S/S* and 2*S/R* Phe-Bx isomers (Fig. 3, bottom). However, only the 2*S/S* isomer is produced in vivo (Fig. 3, center) (Gandía-Herrero et al., 2005b). Since betalamic acid is biosynthesized from L-tyrosine, the absolute configuration of natural betaxanthins is *2S/S*. Spontaneous isomerization to 2*S/R* occurs during semi synthesis (Esteves et al., 2025; Schliemann et al., 1999). A standard curve was then measured (Fig. S2A) and used to determine that Phe-Bx titers on day 5 were just above the calculated limit of detection (LOD) of the Phe-Bx calibration curve (LOD = 0.32 μM/0.11 mg L^{-1}, Fig. S2A). This supports the previous hypothesis that, despite the increase in fluorescence in Fig. 1E, betaxanthins were not detected due to the lack of a dominant betaxanthin species. Phe-Bx titers on day 9 decreased and fell below the LOD. This pattern did not match the observed increase in fluorescence (Fig. 2D). This discrepancy is likely due to the release of small molecules over the course of the growth curve leading to an increase in background fluorescence. It is also possible that other betaxanthin species were formed in small quantities, which were individually not detected by LC-MS, but contributed to the overall increase in fluorescence observed (Fig. 2D).

3.3. High-density cultivation significantly improves betaxanthin yields in Syn-Bx^{AroG*}

We had previously observed that the expression of *aroG*^{fbr} had a negative impact on growth and led to an early entrance into stationary phase in Syn-Bx^{AroG*} (Fig. S6A). This is likely due to the metabolic burden of overproducing multiple amino acids (Brey et al., 2020). Thus, we decided to test whether optimization of the growth conditions could further boost Phe-Bx titers in Syn6803. To this end, we tested cultivation of Syn-Bx^{AroG*} in a nutrient-rich medium with CO_2-enriched air. After induction, the OD, and fluorescence of the culture medium were monitored daily. The control strain Syn-N^{Kan} exhibited strong growth achieving a final OD of 20.7 (Fig. 4A), approximately 3 times higher than in standard growth conditions. The growth of Syn-Bx^{AroG*} matched that of Syn-N^{Kan} until day 3 (Fig. 4A). From then onwards, growth slowed significantly and a final OD of 9.9 was achieved (Figs. 4A), 1.6 times higher than in standard growth conditions. We also measured intra- and extracellular levels of Phe, Tyr, and Trp at days 5, 9, 10, and 11 (Fig. 4B and C) to gain an understanding on how aromatic amino acid availability influenced betaxanthin formation. In the Syn-N^{Kan} strain, the intracellular levels of Phe, Tyr, and Trp were all below the calculated LODs (Fig. S4). On the other hand, the expression of *aroG*^{fbr} led to the detection of intracellular Phe and Tyr up to a maximum of 11.9 and 6.5 μM, respectively (Fig. 4C). It is worth noting that, in Syn-Bx^{AroG*}, Tyr levels remained stable until day 10, suggesting that Tyr was not limiting throughout the experiment. Lower levels of Trp were also detected in Syn-Bx^{AroG*} (1.6–3.3 μM). Analysis of the supernatant showed that Phe was the most abundant amino acid (range of 126.2–680.7 μM) (Fig. 4B). This was followed by Trp (range of 24.7–166.3 μM) and Tyr (range of

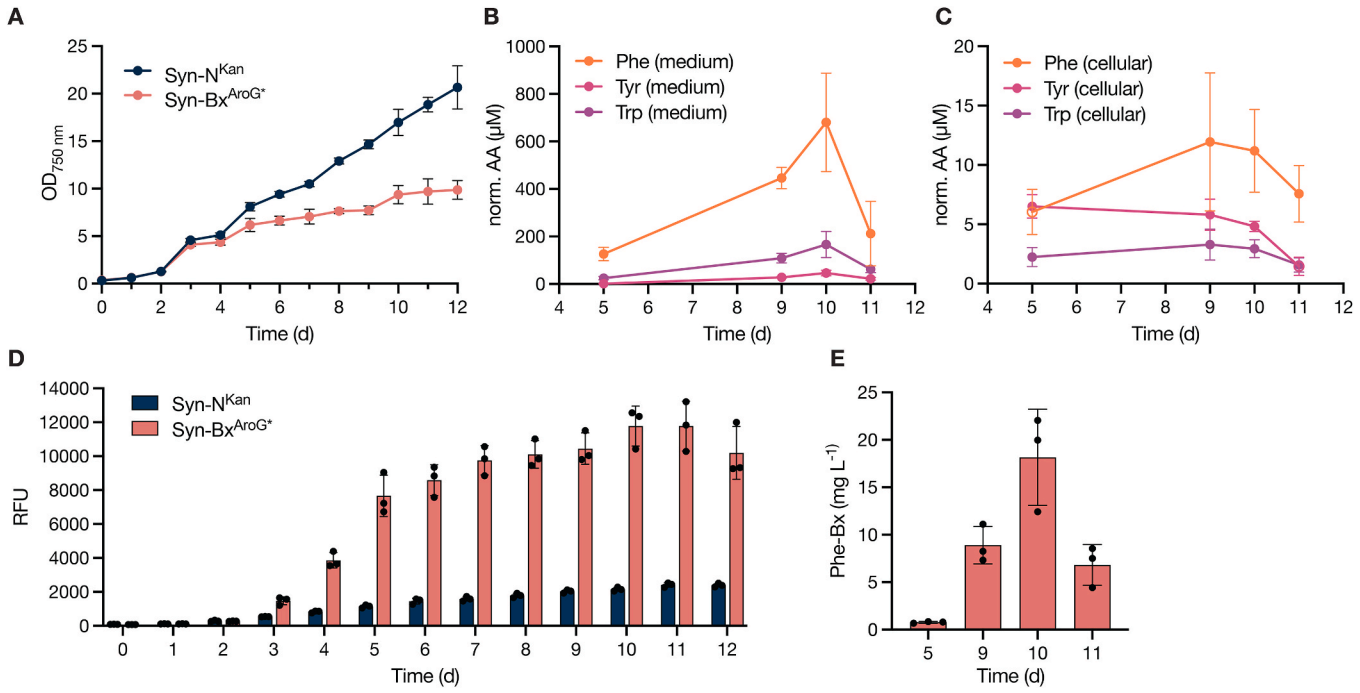


Fig. 4. Betaxanthin production in the Syn-Bx^{AroG*} strain in high density cultivation. **A** Monitoring of growth by measuring OD over 12 days of cultivation at 30 °C with 50 µmol photons m^{-2} s^{-1} in nutrient rich P4-TES CPH medium and high CO_2 conditions supplemented with 50 µg mL^{-1} kanamycin. Cultures of Syn-Bx^{AroG*} and a negative control strain (Syn-N^{Kan}) were induced after 1 day with 1 mg mL^{-1} rhamnose. **B** Phenylalanine (Phe), tryptophan (Trp) and tyrosine (Tyr) content in the culture medium of Syn-Bx^{AroG*} from cultivation day 5, 9, 10 and 11 determined by LC-MS. Amino acid (AA) content in µM was normalized (norm.) to biomass ($OD_{750\ nm}$). **C** Intracellular Phe, Trp and Tyr content in Syn-Bx^{AroG*} from cultivation day 5, 9, 10 and 11 determined by LC-MS. Amino acid (AA) content in µM was normalized (norm.) to biomass ($OD_{750\ nm}$). Open circles denote values that fall within the range of the standard curve but below the limit of quantification. **D** Fluorescence (Ex: 475/15, Em: 515/15) of culture medium measured over 12 days of cultivation. **E** Phe-Bx titers in the culture medium of Syn-Bx^{AroG*} determined by LC-MS using the standard curve in Fig. S2B. All bars and data points in line graphs shown are averages (n = 3), error bars: ±SD.

1.5–46.2 µM).

A significant increase in the Syn-Bx^{AroG*} culture medium fluorescence was observed starting three days after induction ($p = 0.02$). It then continuously increased until day 10 (Fig. 4D). Therefore, intra- and extracellular levels of Phe-Bx were measured by LC-MS at days 5, 9, 10, and 11 (Fig. 4E, S2B). Intracellular analysis showed that the entirety of Phe-Bx was secreted, as none was detected inside the cell. The extracellular analysis showed the volumetric productivity of Phe-Bx rose from 0.77 ± 0.09 mg L^{-1} at day 5 to 18.16 ± 5.1 mg L^{-1} at day 10, after which it decreased significantly at day 11 (Fig. 4E). The decrease in Phe-Bx titers also coincided with a general decrease in intra- and extracellular levels of Phe, Tyr, and Trp. Ultimately, the titer at day 10 represents a 165-times increase in comparison to what was achieved in standard growth conditions.

4. Discussion

In this study we used a beetroot cytochrome P450, CYP76AD1 (variant W13L, F309L), and a L-DOPA dioxygenase, BvDODA1, to establish photoautotrophic betaxanthin pigment biosynthesis in the cyanobacterium *Synechocystis* sp. PCC 6803. Introduction of the feedback-resistant *aroG^{fbr}* together with the betaxanthin pathway led to the detection of Phe-Bx just above the LOD of 0.11 mg L^{-1}. Cultivation in high-nutrient and CO_2 conditions then increased titers approximately 165 times and allowed for the fully photoautotrophic production of Phe-Bx at a titer of 18.2 ± 5.1 mg L^{-1} without exogenous addition of amino acids or ascorbic acid. When comparing the cyanobacterial titers to other efforts to produce Phe-Bx, this value is higher than the 11 mg L^{-1} achieved with a Phe-fed *E. coli* strain expressing a 4,5-DOPA-extradiol-dioxygenase from *Gluconacetobacter diazotrophicus*. The same study achieved higher titers by adding the highly soluble amino acid proline to produce 43 mg L^{-1} Proline-Bx (i.e., indicaxanthin) (Guerrero-Rubio et al., 2019). Our 18.2 ± 5.1 mg L^{-1} Phe-Bx titer is also in the range of the 24 mg L^{-1} of betaxanthins produced with an unmodified CYP76AD1-BvDODA1 pathway in glucose-fed *S. cerevisiae*. Titers in that study rose to 208 mg L^{-1} with extensive transcription factor engineering and cultivation optimization (Xue et al., 2025).

In the present work, the addition of the feedback-resistant *aroG^{fbr}* was crucial for high-titer betaxanthin production. This was likely due to the larger Tyr pool available for CYP76AD1-catalyzed production of L-DOPA (Fig. 4C). Expression of *aroG^{fbr}* also led to the overaccumulation of Phe, Tyr, and Trp in the medium (Figs. 2C and 4B). However, only Phe-Bx was detected. This can be attributed to several factors. First, the accumulation of significantly more Phe than Trp and Tyr. Second, the increased solubility of Phe, which is approximately twice that of Trp and 50 times higher than Tyr (Fleck and Petrosyan, 2014). In the high-density cultivation experiment (Fig. 4), Phe, Tyr, and Trp levels were elevated throughout the experiment until they decreased significantly at day 11. A similar pattern was observed with Phe-Bx titers where the maximum yield was observed at day 10 with a sharp decrease at day 11. Given the excess of amino acids present both intra- and extracellularly (Fig. 4B and C), the Phe-Bx titers may have ultimately been limited by nutrient supply. In the future, this could be addressed by producing betaxanthins in a regime of semi-continuous cultivation with daily harvesting. Given the relative instability of betaxanthins, a higher frequency of product harvesting may also aid in product recovery. Another potential strategy to alleviate the metabolic burden could be based on a two-partner co-cultivation approach: one producing, and secreting, betalamic acid and the second partner secreting an overproduced amino acid for condensation. This was successfully implemented with two *E. coli* strains in co-culture and led to the production of 287.69 mg L^{-1} of histidine-betaxanthin (Hou et al., 2020).

Our work also serves as a foundation for the production of the closely related red-violet betacyanins (Fig. S1). These pigments are more stable,

do not rely on amino acid supply for the condensation reaction and can replace betaxanthins in several applications. This can be achieved by introduction of UDP-glycosyltransferases that can glycosylate the unstable betanidin (product of the condensation of betalamic acid with cyclo-DOPA) to form betanin (Fig. S1). Alternatively, cyclo-DOPA can first be glycosylated by a UDP-glycosyltransferase to form its glucoside, which then condenses with betalamic acid to form betanin (Glitz et al., 2025). The CYP76AD1 variant (W13L, F309L) exhibits a suppressed cyclo-DOPA production pathway. Therefore, either the wild-type CYP76AD1 or a single mutant which promotes betanidin production (CYP76AD1^{W13L}) (DeLoache et al., 2015) would be needed for betacyanin biosynthesis. Betanin would then require only the introduction of appropriate UDP-glycosyltransferases.

Due to their inherent capacity to produce heme-containing proteins, cyanobacteria have become choice organisms for the production of cytochrome P450s. There is the added benefit that membrane-bound plant cytochrome P450s are typically inserted into the thylakoid membranes in cyanobacteria, thus allowing for NADPH-independent light-driven catalysis (Wlodarczyk et al., 2016). If this is also the case with the CYP76AD1 used in this study, then previous synthetic biology strategies to improve cytochrome P450 production, stability, and catalysis could also be applied to betalain biosynthesis. These include improving thylakoid membrane targeting (Hanamghar et al., 2025), fusion of the cytochrome P450 to dedicated electron donors (Mellor et al., 2019; Sutardja et al., 2024), and elimination of competing electron sinks (Spasic et al., 2022; Torrado et al., 2022). From a broader perspective, betalain biosynthesis may also benefit from improvements in metabolic channelling between CYP76AD1 and BvDODA1. This could potentially be achieved by scaffolding of enzymes e.g. on the thylakoid membrane (Behrendorff et al., 2020; Chen et al., 2024).

In conclusion, our work showcases the biosynthetic potential of cytochrome P450-containing pathways in cyanobacteria and opens the door to sustainable production of plant-derived betalain pigments in a microbial host.

CRediT authorship contribution statement

Sayali S. Hanamghar: Writing – review & editing, Writing – original draft, Visualization, Methodology, Investigation, Funding acquisition, Formal analysis, Data curation, Conceptualization. **David A. Russo:** Writing – review & editing, Writing – original draft, Visualization, Supervision, Methodology, Investigation, Formal analysis, Data curation, Conceptualization. **Silas Busck Mellor:** Writing – review & editing, Methodology, Funding acquisition, Formal analysis, Conceptualization. **Julie A.Z. Zedler:** Writing – review & editing, Writing – original draft, Visualization, Supervision, Resources, Methodology, Funding acquisition, Formal analysis, Conceptualization.

Declaration of competing interest

The authors declare no conflict of interest.

Acknowledgements

This work was supported by a PhD scholarship from the Free State of Thuringia granted to SSH, the Deutsche Forschungsgemeinschaft (DFG, German Research Foundation) SFB 1127 ChemBioSys, project number 239748522 (JAZZ, DAR) and the Novo Nordisk Foundation, project number NNF18OC0032350 (SBM). The Exploris 480 mass spectrometer was funded by the Free State of Thuringia (2023 INST 275/535-1 FUGG) and by the Deutsche Forschungsgemeinschaft (DFG, German Research Foundation) project number 529714284.

Appendix A. Supplementary data

Supplementary data to this article can be found online at https://doi.org/10.1016/j.ymben.2026.01.002.

Data availability

The metabolomics data have been deposited to the MetaboLights repository with the study identifier MTBLS12639 and can be accessed via https://www.ebi.ac.uk/metabolights/MTBLS12639. Plasmid maps are available on Zenodo at https://doi.org/10.5281/zenodo.15673972.

References

Abedi-Firoozjah, R., Parandi, E., Heydari, M., Kolahdouz-Nasiri, A., Bahraminejad, M., Mohammadi, R., Rouhi, M., Garavand, F., 2023. Betalains as promising natural colorants in smart/active food packaging. Food Chem. 424, 136408. https://doi.org/10.1016/j.foodchem.2023.136408.

Azeredo, H.M.C., 2009. Betalains: properties, sources, applications, and stability – a review. Int. J. Food Sci. Technol. 44, 2365–2376. https://doi.org/10.1111/j.1365-2621.2007.01668.x.

Babaei, M., Thomsen, P.T., Dyekjær, J.D., Glitz, C.U., Pastor, M.C., Gockel, P., Körner, J. D., Rago, D., Borodina, I., 2023. Combinatorial engineering of betalain biosynthesis pathway in yeast *Saccharomyces cerevisiae*. Biotechnol. Biofuels Bioprod 16, 128. https://doi.org/10.1186/s13068-023-02374-4.

Babos, M., Halász, K., Zagyva, T., Zöld-Balogh, Á., Szegő, D., Bratek, Z., 2011. Preliminary notes on dual relevance of ITS sequences and pigments in *Hygrocybe* taxonomy. Persoonia - Mol. Phylogeny Evol. Fungi 26, 99–107. https://doi.org/10.3767/003158511X578349.

Behrendorff, J.B.Y.H., Borràs-Gas, G., Pribil, M., 2020. Synthetic protein scaffolding at biological membranes. Trends Biotechnol. 38, 432–446. https://doi.org/10.1016/j.tibtech.2019.10.009.

Berepiki, A., Hitchcock, A., Moore, C.M., Bibby, T.S., 2016. Tapping the unused potential of photosynthesis with a heterologous electron sink. ACS Synth. Biol. 5, 1369–1375. https://doi.org/10.1021/acssynbio.6b00100.

Brey, L.F., Włodarczyk, A.J., Bang Thøfner, J.F., Burow, M., Crocoll, C., Nielsen, I., Zygadlo Nielsen, A.J., Jensen, P.E., 2020. Metabolic engineering of *Synechocystis* sp. PCC 6803 for the production of aromatic amino acids and derived phenylpropanoids. Metab. Eng. 57, 129–139. https://doi.org/10.1016/j.ymben.2019.11.002.

Cabanes, J., Gandía-Herrero, F., Escribano, J., García-Carmona, F., Jiménez-Atiénzar, M., 2014. One-step synthesis of betalains using a novel betalamic acid derivatized support. J. Agric. Food Chem. 62, 3776–3782. https://doi.org/10.1021/jf500506y.

Chang, Y.-C., Chiu, Y.-C., Tsao, N.-W., Chou, Y.-L., Tan, C.-M., Chiang, Y.-H., Liao, P.-C., Lee, Y.-C., Hsieh, L.-C., Wang, S.-Y., Yang, J.-Y., 2021. Elucidation of the core betalain biosynthesis pathway in *Amaranthus tricolor*. Sci. Rep. 11, 6086. https://doi.org/10.1038/s41598-021-85486-x.

Chen, Z., Wu, T., Yu, S., Li, M., Fan, X., Huo, Y.-X., 2024. Self-assembly systems to troubleshoot metabolic engineering challenges. Trends Biotechnol. 42, 43–60. https://doi.org/10.1016/j.tibtech.2023.06.009.

Contreras-Llano, L.E., Guerrero-Rubio, M.A., Lozada-Ramírez, J.D., García-Carmona, F., Gandía-Herrero, F., 2019. First betalain-producing bacteria break the exclusive presence of the pigments in the plant kingdom. mBio 10. https://doi.org/10.1128/mbio.00345-19, 10.1128/mbio.00345-19.

DeLoache, W.C., Russ, Z.N., Narcross, L., Gonzales, A.M., Martin, V.J.J., Dueber, J.E., 2015. An enzyme-coupled biosensor enables (*S*)-reticuline production in yeast from glucose. Nat. Chem. Biol. 11, 465–471. https://doi.org/10.1038/nchembio.1816.

Esteves, L.C., Machado, C.O., Gonçalves, L.C.P., Cavalcante, V.F., Obeid, G., Correra, T. C., Bastos, E.L., 2022. Structural effects on the antioxidant properties of amino acid betaxanthins. Antioxidants 11, 2259. https://doi.org/10.3390/antiox11112259.

Esteves, L.C., Pinheiro, A.C., Machado, C.O., Pettigiani, N.B.L., Rodrigues, A.C.B., Taniguchi, M., Lindsey, J.S., Bastos, E.L., 2025. Amino acid betaxanthins: absorption, fluorescence, and stability. J. Nat. Prod. https://doi.org/10.1021/acs.jnatprod.5c00419.

Fleck, M., Petrosyan, A.M., 2014. Salts of Amino Acids: Crystallization, Structure and Properties. Springer International Publishing, Cham. https://doi.org/10.1007/978-3-319-06299-0.

Gandía-Herrero, Fernando, García-Carmona, F., 2012. Characterization of recombinant *Beta vulgaris* 4,5-DOPA-extradiol-dioxygenase active in the biosynthesis of betalains. Planta 236, 91–100. https://doi.org/10.1007/s00425-012-1593-2.

Gandía-Herrero, F., Escribano, J., García-Carmona, F., 2005a. Betaxanthins as pigments responsible for visible fluorescence in flowers. Planta 222, 586–593. https://doi.org/10.1007/s00425-005-0004-3.

Gandía-Herrero, F., Escribano, J., García-Carmona, F., 2005b. Betaxanthins as substrates for tyrosinase. An approach to the role of tyrosinase in the biosynthetic pathway of betalains. Plant Physiol. 138, 421–432. https://doi.org/10.1104/pp.104.057992.

Glitz, C., Dyekjær, J.D., Vaitkus, D., Babaei, M., Welner, D.H., Borodina, I., 2025. Screening of plant UDP-Glycosyltransferases for betanin production in yeast. Appl. Biochem. Biotechnol. 197, 2356–2382. https://doi.org/10.1007/s12010-024-05100-4.

Grützner, R., Schubert, R., Horn, C., Yang, C., Vogt, T., Marillonnet, S., 2021. Engineering betalain biosynthesis in tomato for high level betanin production in fruits. Front. Plant Sci. 12. https://doi.org/10.3389/fpls.2021.682443.

Guerrero-Rubio, M.A., López-Llorca, R., Henarejos-Escudero, P., García-Carmona, F., Gandía-Herrero, F., 2019. Scaled-up biotechnological production of individual betalains in a microbial system. Microb. Biotechnol. 12, 993–1002. https://doi.org/10.1111/1751-7915.13452.

Hanamghar, S.S., Mellor, S.B., Mikkelsen, L., Crocoll, C., Motawie, M.S., Russo, D.A., Jensen, P.E., Zedler, J.A.Z., 2025. Thylakoid targeting improves stability of a cytochrome P450 in the cyanobacterium *synechocystis* sp. PCC 6803. ACS Synth. Biol. 14, 867–877. https://doi.org/10.1021/acssynbio.4c00800.

Hatlestad, G.J., Sunnadeniya, R.M., Akhavan, N.A., Gonzalez, A., Goldman, I.L., McGrath, J.M., Lloyd, A.M., 2012. The beet *R* locus encodes a new cytochrome P450 required for red betalain production. Nat. Genet. 44, 816–820. https://doi.org/10.1038/ng.2297.

Hinz, U.G., Fivaz, J., Girod, P.-A., Zyrd, J.-P., 1997. The gene coding for the DOPA dioxygenase involved in betalain biosynthesis in *Amanita muscaria* and its regulation. Mol. Gen. Genet. MGG 256, 1–6. https://doi.org/10.1007/s004380050539.

Hoschek, A., Toepel, J., Hochkeppel, A., Karande, R., Bühler, B., Schmid, A., 2019. Light-dependent and aeration-independent gram-scale hydroxylation of cyclohexane to cyclohexanol by CYP450 harboring *synechocystis* sp. PCC 6803. Biotechnol. J. 14, 1800724. https://doi.org/10.1002/biot.201800724.

Hou, Y., Liu, X., Li, S., Zhang, X., Yu, S., Zhao, G.-R., 2020. Metabolic Engineering of *Escherichia coli* for de Novo Production of Betaxanthins. J. Agric. Food Chem. 68, 8370–8380. https://doi.org/10.1021/acs.jafc.0c02949.

Jiang, L., Huang, L., Cai, J., Xu, Z., Lian, J., 2021. Functional expression of eukaryotic cytochrome P450s in yeast. Biotechnol. Bioeng. 118, 1050–1065. https://doi.org/10.1002/bit.27630.

Jodlbauer, J., Rohr, T., Spadiut, O., Mihovilovic, M.D., Rudroff, F., 2021. Biocatalysis in green and blue: cyanobacteria. Trends Biotechnol. 39, 875–889. https://doi.org/10.1016/j.tibtech.2020.12.009.

Khan, M.I., 2016. Plant betalains: safety, antioxidant activity, clinical efficacy, and bioavailability. Compr. Rev. Food Sci. Food Saf. 15, 316–330. https://doi.org/10.1111/1541-4337.12185.

Lassen, L.M., Nielsen, A.Z., Olsen, C.E., Bialek, W., Jensen, K., Møller, B.L., Jensen, P.E., 2014. Anchoring a plant cytochrome P450 via PsaM to the thylakoids in *synechococcus* sp. PCC 7002: evidence for light-driven biosynthesis. PLoS One 9, e102184. https://doi.org/10.1371/journal.pone.0102184.

Mascia, F., Pereira, S.B., Pacheco, C.C., Oliveira, P., Solarczek, J., Schallmey, A., Kourist, R., Alphand, V., Tamagnini, P., 2022. Light-driven hydroxylation of testosterone by *Synechocystis* sp. PCC 6803 expressing the heterologous CYP450 monooxygenase CYP110D1. Green Chem. 24, 6156–6167. https://doi.org/10.1039/D1GC04714K.

Mellor, S.B., Vinde, M.H., Nielsen, A.Z., Hanke, G.T., Abdiaziz, K., Roessler, M.M., Burow, M., Motawia, M.S., Møller, B.L., Jensen, P.E., 2019. Defining optimal electron transfer partners for light-driven cytochrome P450 reactions. Metab. Eng. 55, 33–43. https://doi.org/10.1016/j.ymben.2019.05.003.

Myers, J., Graham, J.-R., Wang, R.T., 1980. Light harvesting in *Anacystis nidulans* studied in pigment mutants. Plant Physiol. 66, 1144–1149. https://doi.org/10.1104/pp.66.6.1144.

Polturak, G., Breitel, D., Grossman, N., Sarrion-Perdigones, A., Weithorn, E., Pliner, M., Orzaez, D., Granell, A., Rogachev, I., Aharoni, A., 2016. Elucidation of the first committed step in betalain biosynthesis enables the heterologous engineering of betalain pigments in plants. New Phytol. 210, 269–283. https://doi.org/10.1111/nph.13796.

Polturak, G., Grossman, N., Vela-Corcia, D., Dong, Y., Nudel, A., Pliner, M., Levy, M., Rogachev, I., Aharoni, A., 2017. Engineered gray mold resistance, antioxidant capacity, and pigmentation in betalain-producing crops and ornamentals. Proc. Natl. Acad. Sci. 114, 9062–9067. https://doi.org/10.1073/pnas.1707176114.

Ritchie, R.J., 2006. Consistent sets of spectrophotometric chlorophyll equations for acetone, methanol and ethanol solvents. Photosynth. Res. 89, 27–41. https://doi.org/10.1007/s11120-006-9065-9.

Russo, David A., Zedler, J.A.Z., Jensen, P.E., 2019a. A force awakens: exploiting solar energy beyond photosynthesis. J. Exp. Bot. 70, 1703–1710. https://doi.org/10.1093/jxb/erz054.

Russo, D.A., Zedler, J.A.Z., Wittmann, D.N., Möllers, B., Singh, R.K., Batth, T.S., van Oort, B., Olsen, J.V., Bjerrum, M.J., Jensen, P.E., 2019b. Expression and secretion of a lytic polysaccharide monooxygenase by a fast-growing cyanobacterium. Biotechnol. Biofuels 12, 74. https://doi.org/10.1186/s13068-019-1416-9.

Russo, D.A., Zedler, J.A.Z., Conradi, F.D., Schuergers, N., Jensen, P.E., Mullineaux, C.W., Wilde, A., Pohnert, G., 2022. Development of a highly sensitive luciferase-based reporter system to study two-step protein secretion in cyanobacteria. J. Bacteriol. 204, e00504–e00521. https://doi.org/10.1128/jb.00504-21.

Sadowska-Bartosz, I., Bartosz, G., 2021. Biological properties and applications of betalains. Molecules 26, 2520. https://doi.org/10.3390/molecules26092520.

Schliemann, W., Kobayashi, N., Strack, D., 1999. The decisive step in betaxanthin biosynthesis is a spontaneous reaction. Plant Physiol. 119, 1217–1232. https://doi.org/10.1104/pp.119.4.1217.

Shang, T., Fang, C.M., Ong, C.E., Pan, Y., 2023. Heterologous expression of recombinant human cytochrome P450 (CYP) in *Escherichia coli*: N-terminal modification, expression, isolation, purification, and reconstitution. BioTech 12, 17. https://doi.org/10.3390/biotech12010017.

Spasic, J., Oliveira, P., Pacheco, C., Kourist, R., Tamagnini, P., 2022. Engineering cyanobacterial chassis for improved electron supply toward a heterologous ene-reductase. J. Biotechnol. 360, 152–159. https://doi.org/10.1016/j.jbiotec.2022.11.005.

Spórna-Kucab, A., Tekieli, A., Grzegorczyk, A., Świątek, Ł., Boguszewska, A., Skalicka-Woźniak, K., 2023. Betaxanthin profiling in relation to the biological activities of red and yellow *Beta vulgaris* L. extracts. Metabolites 13, 408. https://doi.org/10.3390/metabo13030408.

Stanier, R.Y., Kunisawa, R., Mandel, M., Cohen-Bazire, G., 1971. Purification and properties of unicellular blue-green algae (order Chroococcales). Bacteriol. Rev. 35, 171–205. https://doi.org/10.1128/br.35.2.171-205.1971.

Sutardja, L., Mellor, S.B., Dodge, N., Matthes, A., Burow, M., Nielsen, A., Jensen, P.E., 2024. Expression of redox partner fusions for light driven cytochrome P450s in the cyanobacterium *synechocystis* PCC. 6803. Synth. Biol. Eng. 2, 10008. https://doi.org/10.35534/sbe.2024.10008.

Timoneda, A., Feng, T., Sheehan, H., Walker-Hale, N., Pucker, B., Lopez-Nieves, S., Guo, R., Brockington, S., 2019. The evolution of betalain biosynthesis in Caryophyllales. New Phytol. 224, 71–85. https://doi.org/10.1111/nph.15980.

Toepel, J., Karande, R., Klähn, S., Bühler, B., 2023. Cyanobacteria as whole-cell factories: current status and future prospectives. Curr. Opin. Biotechnol. 80, 102892. https://doi.org/10.1016/j.copbio.2023.102892.

Torrado, A., Connabeer, H.M., Röttig, A., Pratt, N., Baylay, A.J., Terry, M.J., Moore, C. M., Bibby, T.S., 2022. Directing cyanobacterial photosynthesis in a cytochrome c oxidase mutant using a heterologous electron sink. Plant Physiol. 189, 2554–2566. https://doi.org/10.1093/plphys/kiac203.

Vasudevan, R., Gale, G.A.R., Schiavon, A.A., Puzorjov, A., Malin, J., Gillespie, M.D., Vavitsas, K., Zulkower, V., Wang, B., Howe, C.J., Lea-Smith, D.J., McCormick, A.J., 2019. CyanoGate: a modular cloning suite for engineering cyanobacteria based on the plant MoClo syntax. Plant Physiol. 180, 39–55. https://doi.org/10.1104/pp.18.01401.

Wang, B., Wang, Y., Deng, Y., Yao, Q., Xiong, A., 2024. Synthesis of betanin by expression of the core betalain biosynthetic pathway in carrot. Hortic. Plant J. 10, 732–742. https://doi.org/10.1016/j.hpj.2023.05.012.

Weber, E., Engler, C., Gruetzner, R., Werner, S., Marillonnet, S., 2011. A modular cloning system for standardized assembly of multigene constructs. PLoS One 6, e16765. https://doi.org/10.1371/journal.pone.0016765.

Wlodarczyk, A., Gnanasekaran, T., Nielsen, A.Z., Zulu, N.N., Mellor, S.B., Luckner, M., Thøfner, J.F.B., Olsen, C.E., Mottawie, M.S., Burow, M., Pribil, M., Feussner, I., Møller, B.L., Jensen, P.E., 2016. Metabolic engineering of light-driven cytochrome P450 dependent pathways into *Synechocystis* sp. PCC 6803. Metab. Eng. 33, 1–11. https://doi.org/10.1016/j.ymben.2015.10.009.

Xue, H., Li, M., Cui, Y., Tian, D., Liu, D., Wang, H., 2025. Coordinated synthesis of aromatic amino acid derived pigments in yeast via global transcriptional engineering. Microb. Cell Fact. 24, 174. https://doi.org/10.1186/s12934-025-02799-6.

Yurekten, O., Payne, T., Tejera, N., Amaladoss, F.X., Martin, C., Williams, M., O'Donovan, C., 2024. MetaboLights: open data repository for metabolomics. Nucleic Acids Res. 52, D640–D646. https://doi.org/10.1093/nar/gkad1045.

Zedler, J.A.Z., Schirmacher, A.M., Russo, D.A., Hodgson, L., Gundersen, E., Matthes, A., Frank, S., Verkade, P., Jensen, P.E., 2023. Self-assembly of nanofilaments in cyanobacteria for protein Co-localization. ACS Nano 17, 25279–25290. https://doi.org/10.1021/acsnano.3c08600.